Anisotropic magnetoresistance in polycrystalline $La_{0.67}(Ca_{1-x}Sr_x)_{0.33}MnO_3$

Anisotropic magnetoresistance in polycrystalline $La_{0.67}(Ca_{1-x}Sr_x)_{0.33}MnO_3$

Yiwei Liu[1,2], Zhihuan Yang[1,2], Huali Yang[1,2], Tao Zou[3], Yali Xie[1,2], Bin Chen[1,2], Young Sun[3], Qingfeng Zhan[1,2] and Run-Wei Li[1,2]

[1] Key Laboratory of Magnetic Materials and Devices, Ningbo Institute of Material Technology and Engineering (NIMTE), Chinese Academy of Sciences (CAS), Ningbo 315201, People's Republic of China
[2] Zhejiang Province Key Laboratory of Magnetic Materials and Application Technology, Ningbo Institute of Material Technology and Engineering (NIMTE), Chinese Academy of Sciences (CAS), Ningbo, 315201, People's Republic of China
[3] State Key Laboratory of Magnetism and Beijing National Laboratory for Condensed Matter Physics, Institute of Physics, Chinese Academy of Sciences, Beijing 100080, People's Republic of China

E-mail: zhanqf@nimte.ac.cn and runweili@nimte.ac.cn

Abstract
We investigated the anisotropic magnetoresistance (AMR) effects in polycrystalline $La_{0.67}(Ca_{1-x}Sr_x)_{0.33}MnO_3$. An anomalously large AMR of 19.1% was observed near the metal–insulator transition temperature (T_{MI}) in polycrystalline $La_{0.67}Ca_{0.33}MnO_3$, but slight Sr doping could significantly depress the anomalous AMR around T_{MI}. By studying the temperature, magnetic field, current direction dependence of AMR and the phase transition process, it was suggested that the anisotropic spin-polarized transport and the demagnetization effect together with the metamagnetic transition around T_{MI} play important roles in the anomalous AMR effects in polycrystalline perovskite manganites.

(Some figures may appear in colour only in the online journal)

1. Introduction

Anisotropic magnetoresistance (AMR) is defined as a change in resistance with varying magnetic field direction with respect to a crystal axis or an applied electric current [1]. The AMR effect in conventional ferromagnetic (FM) metals or alloys originates from the spin–orbit coupling effect; the corresponding AMR value is in the order of a few per cent and usually decreases with increasing temperature or decreasing magnetic field [1, 2]. It is well known that perovskite manganites, due to the strong couplings between spin, charge, orbital and lattice, possess a variety of emerging phenomena, such as metal–insulator transition (MIT), colossal magnetoresistance (CMR), charge–orbital ordering (COO), phase coexistence and metamagnetic transition [3, 4]. Recently, an anomalously large AMR with magnitude about two orders larger than that of conventional FM metals or alloys has been found in single crystal manganites [5, 6], which is likely to be caused by the field-tuned MIT. In epitaxial manganite films [7–9], the anomalous AMR was found to be dependent on the lattice constant [10], film thickness [11], crystalline direction [12, 13] and local uniformity [14, 15] due to the strain induced by the lattice mismatch between the films and substrates. Anomalous AMR effects have been observed in polycrystalline bulk manganites as well [16], which suggests that the maximum AMR appearing near T_{MI} is an intrinsic effect related to spin, orbital and lattice couplings [16], but the detailed mechanism for the origin of AMR in polycrystalline manganites is still not well known. Moreover, the enhanced AMR for polycrystalline manganites at low temperatures was attributed to the spin-polarized transport across grain boundaries [16]. Although AMR has been studied in different manganite samples, most of the studies were concentrated on single crystals and epitaxial films. More works are needed to clarify the origin of AMR in polycrystalline manganites. In this paper, we choose polycrystalline $La_{0.67}(Ca_{1-x}Sr_x)_{0.33}MnO_3$ (LCSMO, $0 \leqslant x \leqslant 1$) to study the origin of AMR in polycrystalline manganites, and intend to clarify the influences of demagnetization effect, current direction, phase transition, as well as element doping on AMR in polycrystalline manganites.
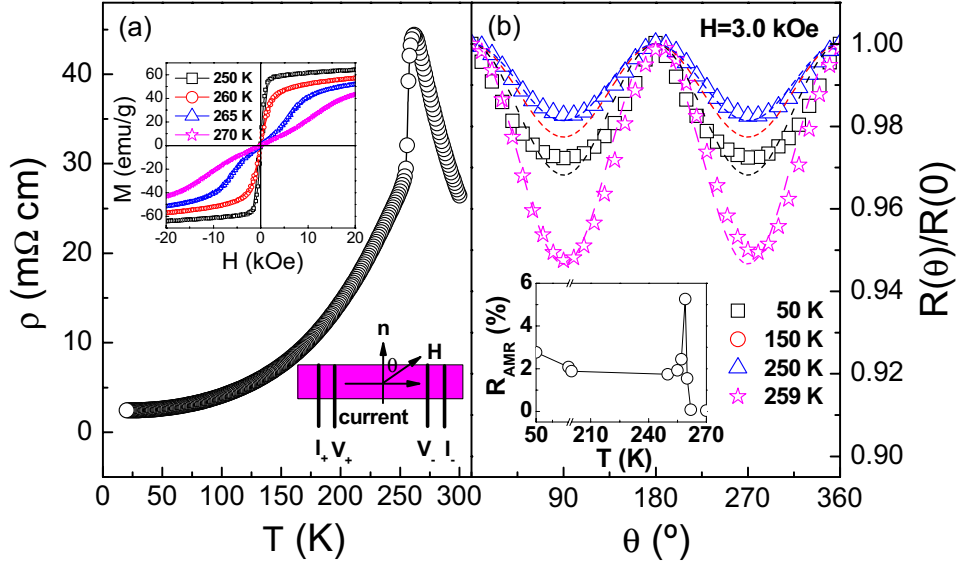
Figure 1. (*a*) Temperature dependence of resistance for polycrystalline LCMO. The upper inset of (*a*) shows the magnetic field dependence of magnetization at various temperatures. The lower inset of (*a*) shows the measuring configuration of the applied field and current. (*b*) Normalized angular dependence of resistance for LCMO at 50, 150, 250 and 259 K. The dashed lines are the fitting lines. The inset of (*b*) shows the temperature dependence of R_{AMR} under a magnetic field of 3.0 kOe.

2. Experimental

Polycrystalline $La_{0.67}(Ca_{1-x}Sr_x)_{0.33}MnO_3$ (LCSMO, $0 \leqslant x \leqslant 1$) samples were synthesized through solid-state reactions from a stoichiometric mixture of high-purity La_2O_3, CaO, $SrCO_3$ and MnO_2. The mixed powders reacted at 1000 °C for 24 h. Then, the resulting powder was ground in an Al_2O_3 crucible and sintered at 1300 °C for 24 h. After repeating this process twice, the powders were pressed to a round sample under a pressure of 20 MPa and were sintered at 1350 °C for 24 h. Finally, the samples were cut into a rectangle shape (8.5 mm × 2.5 mm × 0.7 mm) by a diamond saw. The structures of the polycrystalline $La_{0.67}(Ca_{1-x}Sr_x)_{0.33}MnO_3$ (LCSMO, $0 \leqslant x \leqslant 1$) samples were characterized by x-ray diffraction (XRD). The microstructures were checked by a scanning electron microscope (SEM). The magnetic properties were measured by a vibrating sample magnetometer (VSM) and electron spin resonance (ESR). The magnetotransport properties and their angular dependence were measured by means of a Physical Property Measurement System (PPMS, Quantum Design) with the conventional four-probe technique, as shown in the lower inset of figure 1(*a*). A fixed current of 100 μA was applied between electrodes I_+ and I_-, and the voltages were measured between electrodes V_+ and V_-. During the measurements, the magnetic field (H) was rotated within the sample plane and the resistance was measured as a function of the angle (θ) between H and the in-plane direction (n) along the short edge of the rectangle sample.

3. Results and discussion

The temperature (T) dependence of resistance for the polycrystalline LCMO (LCSMO with $x = 0$) is shown in figure 1(*a*). The critical temperature T_{MI} where dR/dT shows a maximum is obtained at 257 K for the polycrystalline

LCMO. For temperatures above and below T_{MI}, the sample is in paramagnetic (PM) insulating and FM metallic states, respectively. The magnetic field dependence of magnetization is shown in the upper inset of figure 1(*a*). The magnetization is increased linearly with increasing field for $H < 4$ kOe at 265 K, and the slope dM/dH is suddenly increased around $H = 4$ kOe due to the first-order metamagnetic transition from the PM state to the FM state induced by H [17]. The normalized angular dependence of resistances for LCMO at 50, 150, 250 and 259 K under an applied field of $H = 3$ kOe oscillates with a periodicity of 180°, as shown in figure 1(*b*). We tentatively fit the experimental data with a theoretical AMR expression normally used for conventional FM metals [18]:

$$R(\theta)/R(\theta = 0°) = 1 - R_{AMR} \sin^2 \theta, \qquad (1)$$

where R_{AMR} is the AMR amplitude. This expression can nicely fit the data for $T = 250$ K, but fails to describe the results at low temperatures ($T = 50$ and 150 K) and a temperature near T_{MI} ($T = 259$ K), which indicates that the physical origins of AMR in LCMO at low temperatures and around T_{MI} are different from that in conventional FM metals. In fact, the origins of AMR of LCMO are more complicated than those of the conventional FM metals [11, 19]. The temperature dependence of R_{AMR} appears as a peak around T_{MI}, as plotted in the inset of figure 1(*b*). It should be noted that both the maximum value of R_{AMR} and the critical temperature where the R_{AMR} peak appears strongly depend on the magnitude of H. For $H = 3$ kOe, the maximum R_{AMR} is about 5.3% at $T = 259$ K. At low temperatures, the polycrystalline LCMO samples exhibit a significant AMR of about 2%. In contrast, AMR is almost zero in the single crystal and epitaxial thin films of LCMO [7, 8, 11, 19].

The H dependence of R_{AMR} at various temperatures is obtained by measuring the $R-H$ behaviour at the orthogonal
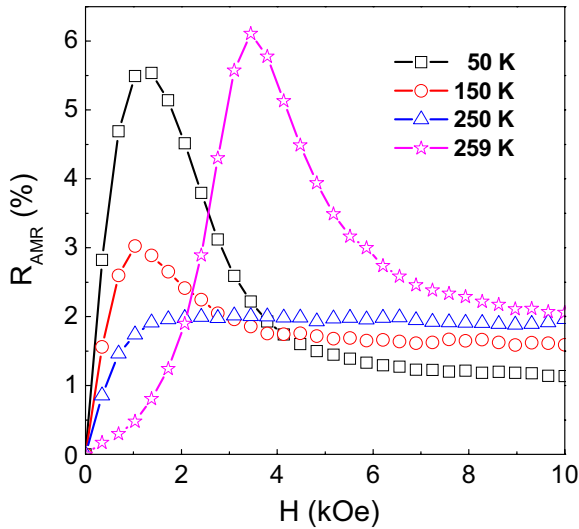
Figure 2. Magnetic field dependence of R_{AMR} at various temperatures.
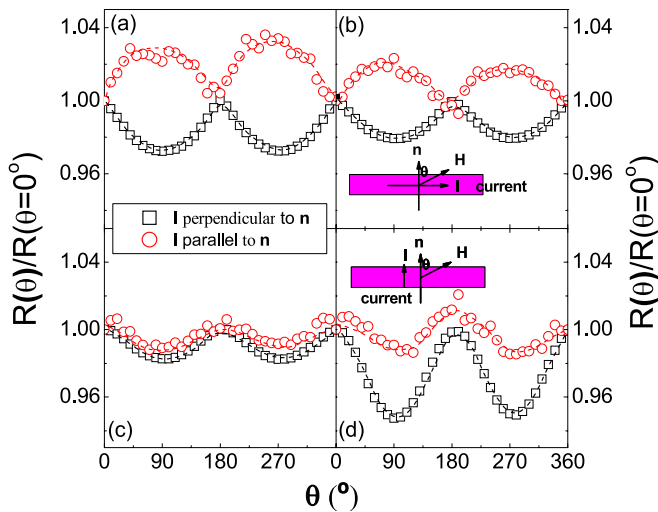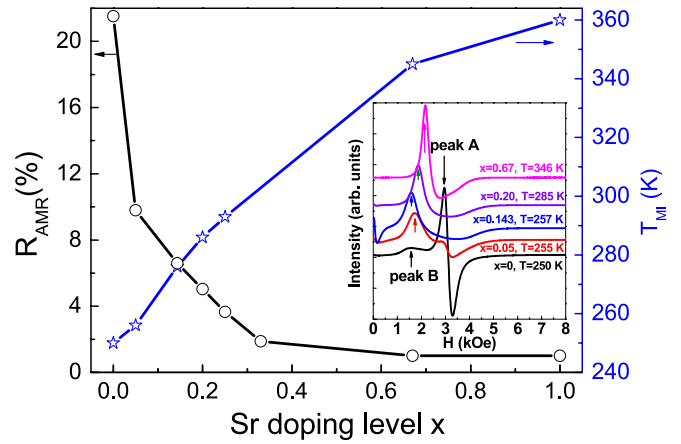

Figure 3. Angular dependence of resistances for current directions along the long and short edges of the samples under $H = 3$ kOe, at (*a*) 50, (*b*)150, (*c*) 250 and (*d*) 259 K. The dashed lines are drawn as a guide to the eye.

Figure 4. R_{AMR} and T_{MI} for LCSMO as a function of Sr content (*x*). The inset shows the ESR spectra for LCSMO with various Sr content *x* near T_{MI}.

Figure 5. XRD spectra of LCSMO with different Sr doping.
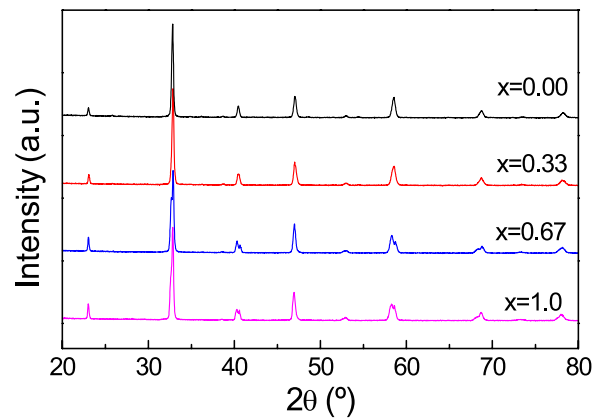
field orientations of $\theta = 0°$ and $90°$, as illustrated in figure 2. The $R_{AMR}-H$ curve appears as a peak at 50 K. With increasing temperature, this peak is reduced and almost disappears at 250 K, but re-emerges close to T_{MI}.

The effect of current orientation on the AMR behaviour of LCMO is studied by comparing the transport properties measured at two orthogonal current directions. When the current direction is varied from $I \perp n$ to $I \parallel n$, the AMR obtained at $T = 50$ and 150 K is changed from negative to positive, as respectively shown in figures 3(*a*) and (*b*). For $T = 250$ K, the AMR remains negative regardless of the current direction, and its ratios are almost identical for the two orthogonal current directions, as shown in figure 3(*c*). When the temperature approaches T_{MI}, the AMR remains negative but the amplitude changes, as shown in figure 3(*d*).

The influence of Sr doping on AMR is studied for the LCSMO samples with different Sr doping levels *x*. With

increasing *x* from 0 to 1, T_{MI} is increased from 250 to 360 K, but the maximum value of R_{AMR}, which occurs near T_{MI}, drops drastically from 19.1% to 1.0%, as plotted in figure 4. The XRD results for LCSMO, as shown in figure 5, indicate a structure change from orthorhombic (*Pbnm*) to rhombohedral (*R*-3*c*) symmetry with increasing Sr content, but this structure change seems to have no impact on the AMR value obtained around T_{MI}. When the crystal structure is changed from orthorhombic symmetry (with Sr content of 33%) to rhombohedra (with Sr content of 67%), the variation of AMR value is very small, as shown in figure 4. Since our samples are polycrystalline, the orientations of the crystal lattices are randomly distributed. Therefore, the influence of the crystal structure on AMR may compensate for each other. In order to investigate the relationship between AMR and the phase coexistence, ESR measurements were conducted in a field-sweeping mode for LCSMO with different *x* near T_{MI}, as shown in the inset of figure 4. Peak A corresponds to the PM phase with Lande *g*-factor of 2.0, which is almost independent of the temperature. Peak B indicating the FM phase is shifted to a low field with decreasing temperature. The coexistence of peaks A and B for $x = 0$ and 0.05 indicates an occurrence of coexistence of FM and PM phases. When $x \geqslant 0.143$, only peak B can be detected, which suggests that the effect of phase coexistence is significantly depressed.
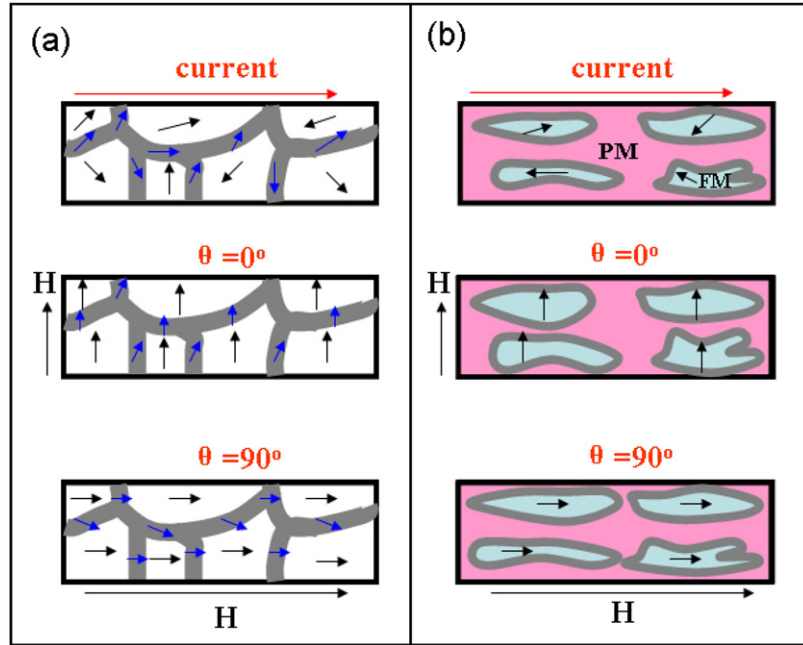
Figure 6. (*a*) Models for anisotropic spin-polarized transport at low temperatures. (*b*) Models for anisotropic magnetotransport with phase coexistence around T_{MI}.

The different types of AMR behaviour in LCMO in various temperature ranges can be understood by considering anisotropic spin-polarized transport, metamagnetic transition, phase coexistence and demagnetization effects. First, when the temperature is low ($T = 50$ and 150 K), AMR behaviour can be interpreted using a theoretical model based on the anisotropic spin-polarized transport across the grain boundaries proposed by Xu *et al* [20]. In experiments, SEM images (not shown) indicate that the grain size for our samples with different Sr doping values is in the order of micrometres. In the absence of H, the magnetization direction of each FM grain is randomly oriented. Under a moderate H, the magnetization of LCSMO grains is aligned, as schematically shown in figure 6(*a*) [19]. The local field induced by the aligned grains partially reduces H at the sidewalls between one grain and the neighbouring one, but enhances H between the north pole of one grain and the south pole of the other grain. When $\theta = 0°$, the electrons tunnel across the sidewalls, and when $\theta = 90°$, the electrons tunnel between the two poles. The spin configurations for the two types of regions are different, as shown in figure 6(*a*), and the tunnelling probabilities are also different. Consequently, the resistances determined by the tunnelling probabilities of $\theta = 0°$ and $90°$ are different, thus an AMR is induced. After a saturation field is applied, the difference in the spin configurations at the orthogonal magnetic field directions is finally eliminated, and the demagnetization effect induced by the sample shape becomes dominant. R_{AMR} with increasing H first increases to a maximum value due to the anisotropic spin-polarized transport, and then decreases to a constant value caused by the demagnetization effect, as shown in figure 2. Additionally, the anisotropic spin-polarized transport strongly depends on the current direction. When the current direction is along the short edge, the electrons tunnel across sidewalls for $\theta = 0°$, and tunnel between two poles for $\theta = 90°$. However,

when the current direction is applied along the long edge, the electrons tunnel between two poles for $\theta = 0°$, and across sidewalls for $\theta = 90°$. Therefore, when the current direction is rotated by $90°$, the resistivity of $\theta = 0°$ for the new current direction is equal to that of $\theta = 90°$ for the original current direction. In this way, the change in the sign of AMR can be well understood.

With increasing temperature, the spin-polarized transport between LCMO grains is depressed [21] and the demagnetization effect on AMR could not be neglected. The demagnetization effect is only determined by the magnetization for a given shape. With increasing H, the magnetization is increased to a saturation value, and the demagnetization field is also increased to a constant value correspondingly. Therefore, the AMR determined by the demagnetization effect is first increased, and then reaches a saturation value just like the R_{AMR}–H curve for 250 K shown in figure 2. At 250 K, AMR is contributed mainly by the demagnetization effect. Since the demagnetization effect determined by the magnetization is independent of the current direction, both the sign and amplitude of R_{AMR} are independent of the current direction.

When the temperature approaches T_{MI}, LCMO is in a phase-separated state, FM clusters and PM matrix coexist [16]. For the temperature of 259 K slightly higher than T_{MI}, FM clusters could be separated from each other [22]. In this situation, the demagnetization effect is not determined by the shape of the sample, but by the shape of FM clusters, as schematically shown in figure 6(*b*). Therefore, AMR near T_{MI} is determined by the demagnetization effect of FM clusters. For $H = 0$, the magnetization direction of each FM cluster is randomly oriented. Under a moderate H, the magnetization of the FM clusters is aligned, meanwhile some FM clusters become larger and are elongated preferentially along the applied magnetic field, due to the metamagnetic transition [17], as schematically

shown in figure 6(*b*). The current flows through more PM insulating areas for $\theta = 0°$ compared with $\theta = 90°$. Therefore, the resistance of $\theta = 0°$ is higher than that of $\theta = 90°$. When the current direction is rotated by $90°$, the current flows over less PM insulating areas for $\theta = 0°$ compared with $\theta = 90°$, and the resistance of $\theta = 0°$ becomes lower than that of $\theta = 90°$. This means the sign of AMR is changed when the current direction is changed. However, the demagnetization effect of the FM clusters, which is independent of the current direction, is dominant so that the positive AMR does not appear when the current direction is changed.

Our results for LCSMO samples with different Sr doping levels x confirm that the metamagnetic transition and phase coexistence are the key factors for the occurrence of the large AMR near T_{MI}. It is well known that LSMO (LCSMO with $x = 1$) exhibits a second-order magnetic transition but not the metamagnetic transition. From the ESR spectra, it is found that a slight Sr doping can significantly depress the phase coexistence. For $x \geqslant 0.143$, both the phase coexistence and the metamagnetic transition disappear. Correspondingly, the AMR ratio near T_{MI} is drastically decreased with increasing Sr content.

4. Conclusion

The influences of temperature, magnetic field, current direction, demagnetization effect and Sr doping on the anomalous AMR effects were studied in polycrystalline $La_{0.67}(Ca_{1-x}Sr_x)_{0.33}MnO_3$. The results suggest that at low temperatures, the anisotropic spin-polarized transport mainly contributes to the AMR, and this effect is directly correlated with the current direction. When the temperature is near T_{MI}, phase coexistence and metamagnetic transition induced by magnetic field play important roles in the extraordinary AMR effects.

Acknowledgments

References

[1] Rijks Th G S M, Lenczowski S K J, Coehoorn R and de Jonge W J M 1997 *Phys. Rev.* B **56** 362
[2] Herranz G, Sanchez F, Garcia-Cuenca M V, Ferrater C, Varela M, Martínez B and Fontcuberta J 2004 *J. Magn. Magn. Mater.* **272** 517
[3] Dagotto E 2005 *Science* **309** 257
[4] Mira J, Rivas J, Rivadulla F, Vazquez-Vazquez C and Lopez-Quintela M 1999 *Phys. Rev.* B **60** 2998
[5] Li R W, Wang H B, Wang X, Yu X Z, Matsui Y, Cheng Z H, Shen B G, Plummer E W and Zhang J D 2009 *Proc. Natl Acad. Sci. USA* **106** 14224
[6] Ning W, Qu Z, Zou Y M, Ling L S, Zhang L, Xi CY, Du H F, Li R W and Zhang Y H 2011 *Appl. Phys. Lett.* **98** 212503
[7] Donnell J O, Onellion M, Rzchowski M S, Eckstein J N and Bozovic I 1996 *Phys. Rev.* B **54** R6841
[8] Donnell J O, Eckstein J N and Rzchowski M S 2000 *Appl. Phys. Lett.* **76** 218
[9] Bibes M, Laukhin V, Valencia S, Martinez B, Fontcuberta J, Gorbenko O Yu, Kaul A R and Martinez J L 2005 *J. Phys.: Condens. Matter* **17** 2733
[10] Li Q, Wang H S, Hu Y F and Wertz E 2000 *J. Appl. Phys.* **87** 5573
[11] Egilmez M, Patterson R, Chow K H and Jung J 2007 *Appl. Phys. Lett.* **90** 232506
[12] Infante I C, Laukhin V, Sanchez F, Fontcuberta J, Melnikov O, Gorbenko O Yu and Kaul A R 2006 *J. Appl. Phys.* **99** 08C502
[13] Chen Y Z, Sun J R, Zhao T Y, Wang J, Wang Z H, Shen B G and Pryds N 2009 *Appl. Phys. Lett.* **95** 132506
[14] Yau J B, Hong X, Posadas A, Ahn C H, Gao W, Altman E, Bason Y, Klein L, Sidorov M and Krivokapic Z 2007 *J. Appl. Phys.* **102** 103901
[15] Wang L F, Huang Z, Tan X L, Chen P F, Zhi B W, Li G M and Wu W B 2010 *Appl. Phys. Lett.* **97** 242507
[16] Egilmez M, Ma R C, Chow K H and Jung J 2009 *J. Appl. Phys.* **105** 07D706
[17] Li R W, Sun J R, Li Q A, Zhu T, Zhang S Y and Shen B G 2003 *J. Appl. Phys.* **93** 8092
[18] Yuzhelevski Y, Markovich V, Jung G and Gorodetsky G 2011 *J. Appl. Phys.* **109** 063908
[19] Egilmez M, Saber M M, Mansour A I, Ma R C, Chow K H and Jung J 2008 *Appl. Phys. Lett.* **93** 182505
[20] Xu Y H, Dworak V, Drechsler A and Hartmann U 1999 *Appl. Phys. Lett.* **74** 2513
[21] Hwang H Y, Cheong S-W, Ong N P and Batlogg B 1996 *Phys. Rev. Lett.* **77** 2041
[22] Li R W, Wang Z H, Wang W N, Sun J R and Li Q A 2002 *Appl. Phys. Lett.* **80** 3367